I&EC research
Industrial & Engineering Chemistry Research
pubs.acs.org/IECR
Article

Storage Material Effects on the Performance of Ru-Based CO_2 Capture and Methanation Dual Functioning Materials

Alessandro Porta, Roberto Matarrese, Carlo Giorgio Visconti, Lidia Castoldi, and Luca Lietti*

Cite This: *Ind. Eng. Chem. Res.* 2021, 60, 6706−6718
Read Online
ACCESS | Metrics & More | Article Recommendations | Supporting Information

ABSTRACT: In this study, a systematic investigation on Dual Functioning Materials (DFMs) for the capture and methanation of CO_2 is carried out. The attention is focused on the nature of the CO_2 adsorbent component (storage material, SM) varying between alkaline (Li, Na, K) and alkaline-earth (Mg, Ca, Ba) metal oxides in combination with Ru, both supported on an Al_2O_3 support. Combining gas phase reactivity analysis and FT-IR characterization, the samples are characterized in terms of CO_2 storage capacity. It is found that all the SM-containing samples adsorb significant amounts of CO_2 as carbonate species, with the higher amounts being adsorbed when the more thermally stable species are formed, i.e., when Ca, Ba, or K are employed as SMs. In all cases, the hydrogenation of the adsorbed carbonates to CH_4 occurs at lower temperature, if compared to their thermal desorption. However, in the case of Ca- and Ba-based DFMs, resilient carbonates are present on the material surface. It was found that the SMs able to form the more thermally stable carbonates upon CO_2 adsorption also showed the best performances in capture/methanation cycles at 350 °C, even if some residual carbonates were left on the DFM after the hydrogenation step. In particular, the following order of reactivity has in fact been observed in terms of CH_4 production: Ru−K ≥ Ru−Ba > Ru−Ca > Ru−Na ≫ Ru−Mg ≅ Ru−Li ≅ Ru. The presence of steam and O_2 during the capture step has a detrimental effect on the CO_2 adsorption for all samples and, as a result, on CH_4 production due to the competition of CO_2 and water for the same adsorption sites. Thus, only SMs able to form strongly bound carbonates species upon CO_2 exposure can retain significant CO_2 storage capacity also in the presence of water in the adsorption feed.

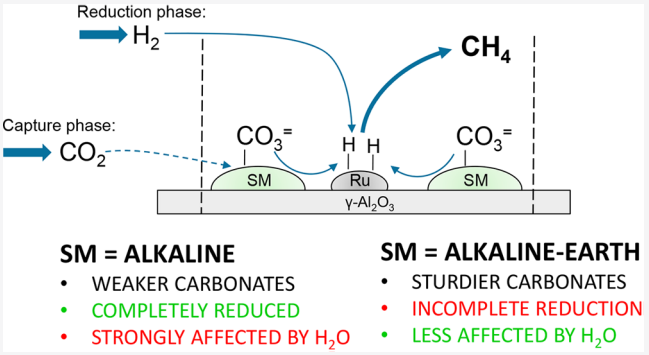

1. INTRODUCTION

CO_2 concentration in the atmosphere has been steadily increasing as a result of the emissions required from the increasing global energy demand.[1] This is associated with the dreadful phenomenon of climate change,[2] and all efforts must be made in order to reduce CO_2 emissions. In this context, carbon capture is expected to play an important role, together with an increase in the efficiency of industrial processes and with a large deployment of renewable energies.[1,3]

Currently, CO_2 is mainly separated using adsorption processes relying on organic amine liquid solutions or solid materials such as metal oxides or molecular sieves.[4] Both processes rely on a thermal swing in order to release CO_2 and regenerate the adsorbent, lowering the overall efficiency of the process. Furthermore, once CO_2 has been desorbed, it needs to be stored away (CCS) or put to use (CCU).

An elegant solution coupling carbon capture and carbon utilization has been proposed and patented in recent years under the name of Dual Functioning Materials (DFMs).[5,6] The envisioned application of these materials is to cyclically capture CO_2 from combustion flue gases after pollutant abatement (e.g., particulate, SO_x, NO_x) and to hydrogenate the captured CO_2 to produce a fuel while regenerating the adsorbent. More specifically, DFMs should be designed to selectively capture CO_2 from steam- and O_2-containing flue gases at relatively high temperatures (300−350 °C); after CO_2 adsorption, they are exposed to a (renewable) H_2-containing stream producing carbon neutral CH_4 while regenerating the adsorbent at the same temperature.[7,8] The overall adsorption−hydrogenation process follows the stoichiometry of the Sabatier reaction 1:

$$CO_2 + 4H_2 \rightarrow CH_4 + 2H_2O \quad (1)$$

Since both adsorption and methanation steps are exothermic processes, external energy inputs are not required. The same technology has also been proposed for dry reforming reactions, though in these cases the CO_2 reduction process is endothermic and occurs at much higher temperatures, thus requiring a high energy consumption.[9]

Special Issue: Enrico Tronconi Festschrift

Received: November 30, 2020
Revised: March 4, 2021
Accepted: March 4, 2021
Published: March 31, 2021

DFMs require the presence of a storage material to selectively adsorb CO_2 and of a methanation catalyst to activate H_2 and reduce CO_2.[5] Even though the storage material and methanation catalyst can be supported on different particles, it has been shown that dispersing both metals on the same support increases the methane production during isothermal operations.[5,10]

Ru, with loadings in the range 1−5 wt %,[10−13] is typically used as methanation catalyst due to its easy reducibility and high methanation activity.[14] Rh at 1 wt % showed improved performances with respect to 5 wt % Ru for DFM applications, but it was ruled out due to economic concerns.[15] Ni, the most used methanation catalyst for Power-to-Gas (PtG) applications,[16] can also be used, but its use in DFM formulations for flue gas applications is hindered by its poor reducibility, making its application feasible only in the presence of noble metal promoters.[17]

A wide variety of metals has been proposed as CO_2 storage material in DFM formulations. A 10% Na_2CO_3/5% Ru/Al_2O_3 material was cycled 50 times at 300 °C under simulated flue gas conditions (7.5% CO_2, 4.5% O_2, 15% H_2O, balance N_2) exhibiting stable behavior, with a CO_2 adsorption capacity of 400 μmol/g_{cat} and a CH_4 production of 320 μmol/g_{cat} when exposed to 15% H_2/N_2 for 15 min.[11] A 10% CaO/5% Ru/Al_2O_3 sample was subject to 20 cycles at 320 °C in the presence of 8% CO_2, 21% H_2O, and balance air, with an average CH_4 production of 283 μmol/g_{cat} per cycle when exposed to 4% H_2/N_2 for 45 min.[5] A small decrease in CH_4 was observed in the latter case and was attributed to the sintering of both Ru and CaO particles. A 16% Ba/1% Ru/Al_2O_3 material mimicking a Lean NO_x Trap (LNT) catalyst composition was used by us to investigate the role of the proximity between Ru and the storage component.[10] This sample was cycled at 350 °C in the presence of a 1% CO_2, 2.5% H_2O and 3% O_2 during the adsorption step and demonstrated an adsorption capacity of 165 μmol/g_{cat} and a CH_4 formation of 80 μmol/g_{cat} when exposed to 4% H_2/He for 10 min.

Other alkaline or alkaline-earth metals have been proposed as storage materials for DFM applications, but to the best of our knowledge they have not been tested in the presence of O_2 and H_2O so far. This is indeed a key aspect for flue-gas applications in view of the presence of relevant amounts of O_2 and H_2O in the combustion effluents (roughly 3% O_2 and 18% H_2O v/v in the case of natural gas combustion).

Arellano-Treviño et al.[15] compared the performance of Na-, K-, Ca-, and Mg-based DFMs with 5 wt % Ru on Al_2O_3 and concluded that the best formulation includes Na as storage material. Based on TGA and cyclic experiments, 10 wt % MgO was ruled out due to its poor CO_2 adsorption capacity at 320 °C while 10 wt % K_2CO_3 and 10% CaO were ruled out due to the long time required to completely hydrogenate the adsorbed carbonates at 320 °C. It was speculated that the different performance derived from the different adsorption modes of CO_2 on the storage materials: the adsorption at 320 °C is too weak in the case of Mg and too strong in the case of Ca and K, leading to poor CO_2 adsorption in the first case and to incomplete hydrogenation of the adsorbed species in the latter. Similar conclusions using the same storage materials but using Ni (instead of Ru) as methanation catalysts have been reported.[18]

Bermejo-López et al. published similar observations regarding the stability of the adsorbed species based on temperature-programmed and cyclic experiments on Na- and Ca-based DFM with a Ru loading of 4%[12] or with a Ni loading of 10%.[19] Interestingly, the Ca-based DFM showed a higher CH_4 selectivity during cycles, with the Na-based DFM producing more CO.

Cimino et al. investigated different alkaline metals (1.7% Li, 4.3% Na, and 5.7% K) coupled with 1 wt % Ru and concluded that Li shows the best performances during methanation cycles ad 230 °C, in terms of both faster methanation kinetics and higher methane production.[13] Sun et al. recently proposed a 6.6% Ru/CeO_2 methanation catalyst mixed in a 1:2 ratio by weight with a MgO bulk adsorbent promoted with Li, Na, and K, corresponding to an overall sorbent content of 67% by weight.[20] This formulation exhibited a staggering CH_4 yield of 6.6 mmol/g_{MgO} when cycled at 300 °C with 65% CO_2/N_2 and 4% H_2/N_2. However, 50% of its reported methane formation was lost in 10 cycles due to the sintering of the MgO adsorbent and the duration of the reduction phase during cycles is in the order of hours and not reported explicitly, making comparisons with literature data difficult.

Given these premises, this work aims at providing a straightforward comparison of several alkaline and alkaline-earth storage materials (SM) using a 1 wt % Ru/Al_2O_3 methanation catalyst doped with the same molar amounts of storage material to maintain the same SM/Ru molar ratio. The comparison is carried out by temperature-programmed experiments and cyclic tests, in absence and in the presence of O_2 and H_2O during the adsorption step, mimicking flue-gas applications. This is in fact a key point in view of the potential application of such materials under real conditions. The reactivity study has been coupled with FT-IR characterization studies on selected samples to get information on the reaction pathways, and results are given below.

2. EXPERIMENTAL SECTION

2.1. Catalyst Preparation and Characterization.

Commercial γ-Al_2O_3 microspheres (Sasol Puralox, 75−100 μm) were used as support. Ru (1 wt %) was introduced by impregnation starting from a commercial $Ru(NO)(NO_3)_3$ solution (Alfa Aesar, 1.5% g_{Ru}/mL). The impregnation was carried out by pouring on the support a Ru solution having the required Ru amount to obtain the 1% w/w Ru sample, with a total volume that is 1.5 times higher than the support pore volume.[21] A slurry is thus obtained; after stirring at room temperature until incipient wetness conditions are reached, the sample is dried overnight at 120 °C in static air. The nitrosyl-nitrate precursor is decomposed in 5% H_2/N_2 at 400 °C for 3 h (5 L(STP)/h/g_{cat}, $T_{ramp\text{-}up}$ = 2 °C/min) and passivated in 2% O_2/He at room temperature (1 L(STP)/h/g_{cat}).

The storage materials (SMs) were introduced on the prepared passivated 1% Ru/Al_2O_3 catalyst by incipient wetness impregnation starting from the corresponding acetate salt (lithium acetate dihydrate, >98%, Sigma-Aldrich; sodium acetate anhydrous, >99%, Merck; potassium acetate anhydrous, >99%, Sigma-Aldrich; calcium acetate monohydrate, >99%, Sigma-Aldrich; barium acetate anhydrous, >99%, Sigma-Aldrich), with the exception of Mg (magnesium nitrate exahydrate, >99%, Acros Organics). The impregnation order was chosen to replicate prior literature on LNT catalysts with similar formulations.[22,23] The impregnated Ru−SM/Al_2O_3 samples were dried overnight at 80 °C in static air and activated at 500 °C in the reactor (see below).

https://doi.org/10.1021/acs.iecr.0c05898
Ind. Eng. Chem. Res. 2021, 60, 6706−6718

Table 1. Nominal Compositions, Morphological Characterizations, and Preliminary Performance Data of the Prepared Samples

sample	Al_2O_3	Ru	Ru−Li	Ru−Na	Ru−K	Ru−Mg	Ru−Ca	Ru−Ba
nominal Ru loading [wt %]	0	1	0.99	0.97	0.95	0.97	0.95	0.84
nominal SM loading [wt %]	0	0	1.0	3.0	5.0	3.2	5.1	16.0
S_{BET} [m^2/g]	191	182	172	155	136	145	136	126
V_p [cm^3/g]	0.5	0.46	0.45	0.43	0.37	0.43	0.37	0.32
$d_{p,avg}$ [nm]	10	10	10	10	9	9	10	10
T_{20} [°C][a]	>500	291	309	338	320	338	329	362
CO_2 desorbed during CO_2-TPD [μmol/g]	68	73	121	223	418	147	350	402
CO_2 desorbed during H_2-TPSR [μmol/g]	69	40	78	107	242	93	110	153
CH_4 produced during H_2-TPSR [μmol/g]	0	27	52	133	249	67	315	305

[a]Temperature corresponding to 20% CO_2 conversion during cofeeding tests.

The nominal metal loadings of the different storage materials are reported in Table 1 and have been set to obtain in the DFM a constant molar amount of SM, yielding a constant SM/Ru ratio of ∼14. All DFMs were prepared starting from the same 1% w/w Ru/Al_2O_3 sample; however, due to the different % w/w SM loadings, the final Ru nominal content differs in each DFM sample. Each sample will be recalled in the text and captions throughout the paper using only the active elements deposited on the Al_2O_3 support (e.g., Ru for Ru/Al_2O_3 and Ru−SM for $Ru-SM/Al_2O_3$).

A Micromeritics Tristar 3000 instrument was used to obtain N_2 physisorption isotherms at its normal boiling point and calculate the Brunauer−Emmett−Teller (BET) surface area (S_{BET}), pore volume (V_p), and average pore diameter ($d_{p,avg}$). All $Ru-SM/Al_2O_3$ samples were characterized after the acetate precursor decomposition procedure, described below. Each sample was degassed for 3 h at 120 °C before N_2 adsorption and after the acetate decomposition.

2.2. Catalyst Testing. All tests were carried out using 60 mg of dried sample, sieved to 140−200 mesh and loaded in a quartz microreactor with an internal diameter of 8 mm. The temperature is controlled using a K-type thermocouple located in the center of the catalytic bed. A bed of quartz granules is present above the catalytic bed to reduce the volume of the reactor and properly mix the feed gases.

The outlet gases were monitored with a Pfeiffer QMS200 quadrupole mass spectrometer, a MKS Multigas 2030 FT-IR spectrometer, and an Agilent 3000 micro gas chromatograph. All tests were carried out with an inlet flow rate of 100 mL(STP)/min, resulting in a space velocity of 100 L(STP)/h/g_{cat}. More detailed information on the experimental setup are available elsewhere.[10]

Prior to catalytic testing, each sample was pretreated in situ to decompose the SM precursor salt. The decomposition was carried out in He flow at 500 °C for 30 min (heating rate: 10 °C/min). The sample was then cooled down to 100 °C and reduced in 4% H_2/He to 500 °C for 1 h (heating rate: 10 °C/min). The activation temperature was selected to be higher than that adopted during the experiments. During both the He and H_2 pretreatment, the effluents were monitored to evaluate the extent of the precursor decomposition. Both in the case of the acetate and nitrate SM precursors complete decomposition/reduction of the precursors was observed, possibly leading to the formation of the corresponding carbonates, oxides/hydroxides species, as indeed showed by FT-IR measurements in the case of the Ba and K SMs.

All samples were characterized at first in terms of methanation reactivity (by CO_2/H_2 cofeeding tests) and in terms of stability and reactivity of CO_2 adsorbed species (by CO_2-TPD and H_2-TPSR after CO_2 adsorption). In particular, CO_2/H_2 cofeeding tests were performed by feeding a flow containing 1% CO_2 and 4% H_2 (He balance) at 100 °C, followed by heating to 500 °C at a rate of 10 °C/min to investigate the reactivity of the systems in the Sabatier reaction.

The stability and reactivity of the adsorbed CO_2 species was investigated after exposure of the reduced samples to 1% CO_2 in He at 500 °C, followed by a temperature decrease to 100 °C (cooling rate: 5 °C/min) while keeping the CO_2 flow. According to this procedure, it is expected to maximize the amount of CO_2 adsorbed on the sample. After 10 min at 100 °C, the CO_2 flow was switched off, and after stabilization of the analyzer signals the temperature was increased to 500 °C in He (CO_2-TPD) or in 4% H_2/He (H_2-TPSR). Quantitative evaluation of the evolved species was obtained by integration of the concentration profiles of the species evolving during the temperature programming tests versus time, according to eq 2:

$$\left[\frac{\mu\text{mol}_i}{g_{cat}}\right] = \int C_i \, dt \, \frac{Q}{22.414} \, \frac{1}{g_{cat}} \tag{2}$$

where g_{cat} refers to the amount of fresh catalyst loaded in the reactor, C_i is the concentration of the i-species measured during the run (ppm), t is the time (s), and Q is the total volumetric flow rate measured at 273 K and 1 atm (Ls^{-1})

CO_2 capture and methanation cycles were performed at 350 °C. Each cycle was composed of (i) CO_2 capture, (ii) inert purge, (iii) methanation with H_2, and (iv) inert purge. The capture step was carried out by exposing the sample to a 1% CO_2/He stream for 10 min, the methanation step by exposing the sample to a 4% H_2/He stream for 10 min. Several cycles were repeated to ensure reproducible results. After cyclic operations, the temperature was increased to 500 °C (TPR, heating rate: 10 °C/min) to clean the catalyst surface.

The presence of H_2O and O_2 during the capture phase was also investigated by adding 3% O_2 and 2.5% H_2O to the CO_2-containing stream. O_2 was fed together with CO_2 using 4-way pulse valves, while water was fed by saturating the He carrier with water vapor. The saturated carrier was fed into the reactor 2 min earlier and removed 2 min after the CO_2/O_2 mixture to ensure the full hydration of the sample.

FT-IR spectra were run on a Nicolet Nexus Fourier Transform instrument equipped with a DTGS detector with a resolution of 4 cm^{-1} (number of scans 20). Powder samples were compressed in self-supporting discs (of about 15 mg, diameter = 13 mm) and placed in a commercial heated stainless-steel cell (ISRI Infrared Reactor, Granger, IN, USA)

https://doi.org/10.1021/acs.iecr.0c05898
Ind. Eng. Chem. Res. 2021, 60, 6706−6718

allowing thermal treatments in situ under vacuum or controlled atmosphere. CO_2-TPD, H_2-TPSR, and CO_2 capture/methanation cycles were carried out on Ru−K and Ru−Ba samples. The adsorption of CO_2 (5 mbar) was performed in the range 375−100 °C. CO_2-TPD and H_2-TPSR were then performed by heating under vacuum conditions and in the presence of H_2 (40 mbar) in the range 100−375 °C (10 °C/min). CO_2 capture and methanation cycles were performed at 350 °C by alternating CO_2 storage (5 mbar) and H_2 (40 mbar), respectively. Before all the measurements, the samples were pretreated at 375 °C in H_2 (100−300 mbar). In the figures, spectra are reported as difference spectra, where the subtrahend spectrum is that of the sample after the activation.

3. RESULTS AND DISCUSSION

3.1. Materials Characterization. Table 1 reports the morphological characterization of the prepared DFM catalysts. The specific surface area of the Al_2O_3 support slightly decreases upon addition of Ru, and more clearly with the subsequent addition of the SMs. In particular, in both the alkaline and alkaline-earth series the values of the surface area decrease upon increasing the molecular weight of the SM (from 172 to 136 m^2/g in the Li−Na−K series, and from 145 to 126 m^2/g in the Mg−Ca−Ba series), along with the pore volume. At variance, the pore diameter remains almost constant for all the prepared materials, near 10 nm. These results can be explained by suggesting that the SM added to the Ru/Al_2O_3 sample does not contribute to the surface area, i.e. it is not porous. In fact, the observed decrease of the surface area upon addition of the SM is consistent (or slightly higher) with the amount of SM added (considered in the form of carbonate, as expected after calcination). This also explains the decrease of the pore volume, while the pore radius keeps constant. Additional pore blocking phenomena upon addition of the SM can also be invoked to account for the slightly higher decrease of the surface area if compared to that expected upon addition of the nonporous SM.

The activity of the prepared DFM has been characterized by cofeeding CO_2 (1% v/v) and H_2 (4% v/v) under temperature programming from 100 to 500 °C. The results are shown in Figure S1 of the Supporting Information in terms of CO_2 conversion and CH_4 selectivity. Table 1 reports for each sample the temperature corresponding to a CO_2 conversion of 20% (T_{20}) during the cofeeding tests, taken as representative of the catalyst activity. The highest CO_2 conversion and CH_4 selectivity is observed in absence of SM, with the Ru sample reaching 20% of CO_2 conversion below 300 °C with CH_4 as main reaction product below 450 °C.

Whenever a SM is present, a decrease in CH_4 yield is observed because of a decrease in both activity and selectivity, with CO as main reaction product. The effect of both alkaline and alkaline-earth components in the methanation reaction has been well documented in the literature.[8] If such metals are present in low amounts the effect on the methanation activity is beneficial because they increment the basicity of the support. However, if such materials are present in higher amounts (like those required to have a significant CO_2 storage capacity for DFM applications), they hinder the methanation activity. This is due both to an electronic effect as well as a masking effect of the Ru sites by the basic promoter.

By comparing the T_{20} reported in Table 1, the activity order proceeds as follows Ru > Ru−Li > Ru−K ≥ Ru−Ca ≥ Ru−Mg = Ru−Na > Ru−Ba. Please note that as the comparison has been carried out loading the same amount of DFM in the reactor (i.e., 60 mg, including the weight of the SM-precursor), the lowest performance of Ba can partially be ascribed to the lower Ru amount present on the sample (0.84% w/w) due to the heavy weight of the alkaline-earth metal.

3.2. CO_2-TPD Tests. CO_2-TPD tests were carried out to gather information on the thermal stability of the adsorbed species when exposing each sample to a CO_2-containing stream as detailed in the Experimental Section. The CO_2 evolution recorded upon heating each sample to 500 °C with preadsorbed CO_2 is shown in Figure 1, and the corresponding amounts are reported in Table 1. In all cases, CO_2 is the only C-containing species evolving from the samples.

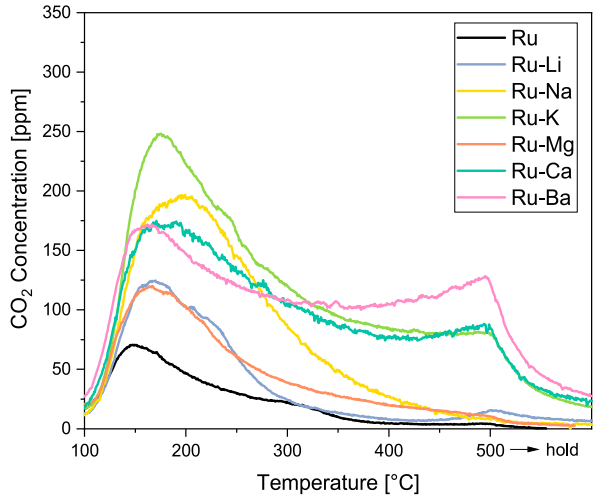

Figure 1. CO_2-TPD profiles on 60 mg of the prepared samples. CO_2 preadsorption conditions: 1% CO_2/He while decreasing temperature from 500 to 100 °C (cooling rate: −5 °C/min). Heating to 500 °C at 10 °C/min in He.

On the Ru sample, the CO_2 desorption profile shows a broad peak with a maximum at 150 °C. This is likely related to bicarbonate species adsorbed on the Al_2O_3 support,[24] as the presence of 1% Ru does not significantly influence the amount of CO_2 adsorbed in the investigated conditions[10,13] (Table 1).

Ru−Li, Ru−Na, and Ru−Mg show a qualitative behavior like that of Ru already described, exhibiting a peak in the 150−200 °C range slowly trailing down at higher temperatures. This indicates that the species arising from CO_2 adsorption on these SMs are characterized by a poor thermal stability.

The integral amount of the desorbed CO_2 is equal to 121 $\mu mol/g_{cat}$ for Ru−Li. This value is considerably lower with respect to 570 $\mu mol/g_{cat}$ obtained for a 1.7% Li/1% Ru/Al_2O_3 sample reported by Cimino et al.[13] The difference can be explained considering the higher Li amount (1.7 vs 1%) and the lower CO_2 adsorption temperature (RT vs 100 °C). Ru−Mg desorbs 147 $\mu mol/g_{cat}$, confirming the poor adsorption capacity of Mg for this application.[25] The Ru−Na sample desorbs 223 $\mu mol/g_{cat}$, which is well in line with the 225 $\mu mol/g_{cat}$ desorbed in similar conditions from a 4% Ru/5% Na_2CO_3/Al_2O_3 DFM reported in.[12]

Ru−Ca, Ru−K, and Ru−Ba exhibit a more complex desorption profile, with two separate contributions: one centered in the 150−200 °C range and a smaller one peaking at 500 °C, i.e., the maximum investigated temperature of the

https://doi.org/10.1021/acs.iecr.0c05898
Ind. Eng. Chem. Res. 2021, 60, 6706−6718

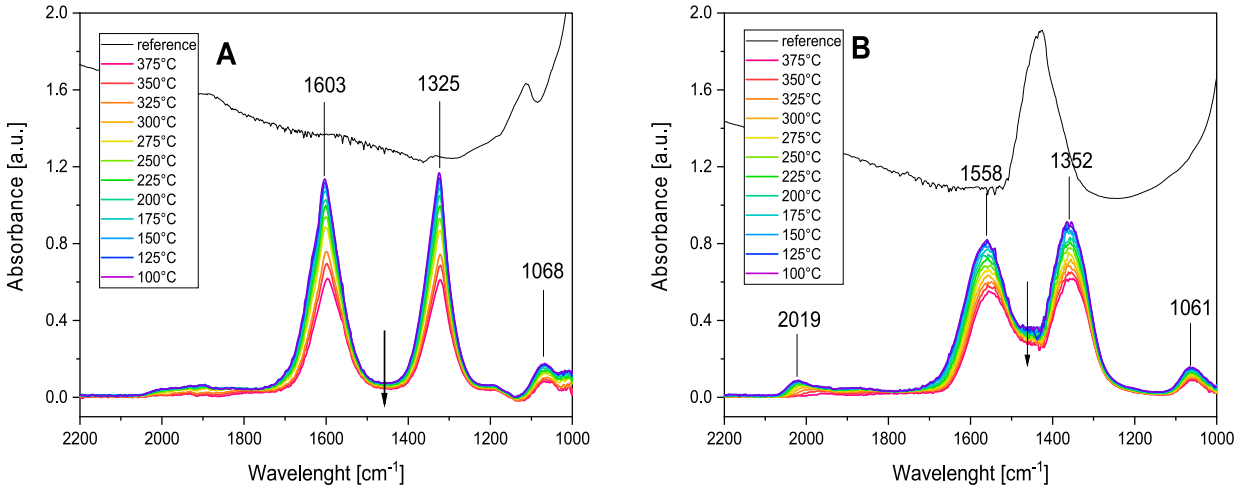

Figure 2. FT-IR spectra during CO_2-TPD on Ru−K (A) and Ru−Ba (B). CO_2 preadsorption conditions: 5 mbar of CO_2 while decreasing temperature from 375 to 100 °C (cooling rate: −5 °C/min). Heating to 375 °C at 10 °C/min in vacuum.

heating ramp. This indicates that different types of adsorbed species are present on these samples, with different thermal stabilities, and that the decomposition of such species is not yet complete at 500 °C, suggesting the presence of species having high thermal stability. These species are likely connected to the formation of stable carbonates arising from the adsorption of CO_2 on large SM agglomerates.[26] As mentioned in the Experimental Section, it is expected that residual carbonates are left on the DFM surface after the acetate precursor decomposition. However, an influence of such species in the high temperature CO_2 desorption feature observed in Figure 1 can be safely ruled out, as a temperature ramp to 500 °C in He was carried out prior to CO_2 adsorption and no CO_2 evolution was observed.

The nature and the thermal stability of species arising from CO_2 adsorption on Ru−K and Ru−Ba samples have been analyzed by FT-IR spectroscopy. For this purpose, the catalysts were saturated upon CO_2 admission at 375 °C, followed by cooling under CO_2 flow at 100 °C. The thermal stability of the species arising upon CO_2 adsorption was investigated upon increasing the temperature from 100 up to 375 °C in vacuum. The results are shown in Figure 2A and B for Ru−K and Ru−Ba samples, respectively. For comparison purpose, in both figures also the background spectrum collected before CO_2 admission and used to obtain the subtracted spectra is reported.

In the case of Ru−K (Figure 2A), CO_2 exposure results in absorption bands centered at 1603, 1325, and 1068 cm^{-1}, which are related to a variety of surface bidentate carbonates (i.e., both chelating and bridged bidentate species) formed on the K phase (i.e., νC═O, ν_{asym} (OCO), and ν_{sym} (OCO) modes).[27] In addition, a minor and very broad spectral feature is observed in the 2050−1800 cm^{-1} spectral region which is related to a variety of carbonyl species on Ru sites in different oxidation states and coordination.[24,28−30] These species are likely formed primarily via r-WGS reaction between CO_2 and residual surface hydrogen from catalyst pretreatment, as the dissociative adsorption of CO_2 on reduced Ru sites is expected to play a minor contribution.[24,31]

Moving to Ru−Ba (Figure 2B), first we emphasize the difference in the background spectrum, if compared to that of Ru−K. Indeed, in the case of Ru−Ba, an intense band at 1440 cm^{-1} characteristic of bulky carbonates has been recognized. These stable species are likely formed on the DFM as a result of the acetate precursor decomposition. The fact that this contribution is almost negligible in the case of the Ru−K sample is in line with the well-known higher stability of the carbonate species arising on barium with respect to potassium.[27,32] Upon CO_2 admission, also in this case, the formation of surface bidentate carbonates adsorbed on the Ba phase is observed (i.e., absorptions at 1558, 1352, and 1061 cm^{-1} assigned to both chelating and bridged species).[27,32−34] In this case, the intensity of the carbonyl related bands in the range 2050−1800 cm^{-1} is significantly enhanced with respect to the case of Ru−K sample. Moreover, the maximum at 2019 cm^{-1} likely suggests that CO is mainly present in the linear configuration on Ru^0 particles.[29,35−37]

Notably, in both cases, no surface species typical of CO_2 adsorption on the alumina support were observed, such as organic-like and hydrogen carbonates that typically form over the alumina surface.[34] The lack of alumina-related CO_2 adsorbed species indicates an extensive spreading of the SM phase covering the support, as also reported elsewhere.[27,33,34]

Upon CO_2 outgassing at increasing temperature, the gradual decrease of surface carbonates is observed which, however, are still present in significant amounts at 375 °C over both samples, and particularly on Ru−Ba. This is in line with the gas-phase results indicating a moderate thermal stability of carbonate species formed upon CO_2 adsorption. Of note, upon heating the high frequency envelopes (i.e., centered 1603 and 1558 cm^{-1}) are also red-shifted to 1598 and 1552 cm^{-1}, respectively. This can be explained by considering that these envelopes result from a variety of strongly overlapped components assigned to chelating and bridged carbonates, the formers more thermally stable,[27] thus giving rise to shifting and less symmetrical bands upon heating.

3.3. Reactivity of adsorbed CO_2 with H_2. H_2-TPSR tests were carried out to probe the reducibility of the adsorbed species arising from CO_2 adsorption. The obtained results are shown in Figure 3 in terms of C-containing species detected (CO_2, CH_4, CO) and total C evolved for each sample (C_{TOT}, i.e. sum of CO_2, CH_4 and CO evolved during each TPSR test). The CO_2 desorption profile recorded during the corresponding CO_2-TPD test is also shown as dotted line. The integral amounts of CH_4 formed and of CO_2 desorbed are reported in Table 1.

https://doi.org/10.1021/acs.iecr.0c05898
Ind. Eng. Chem. Res. 2021, 60, 6706−6718

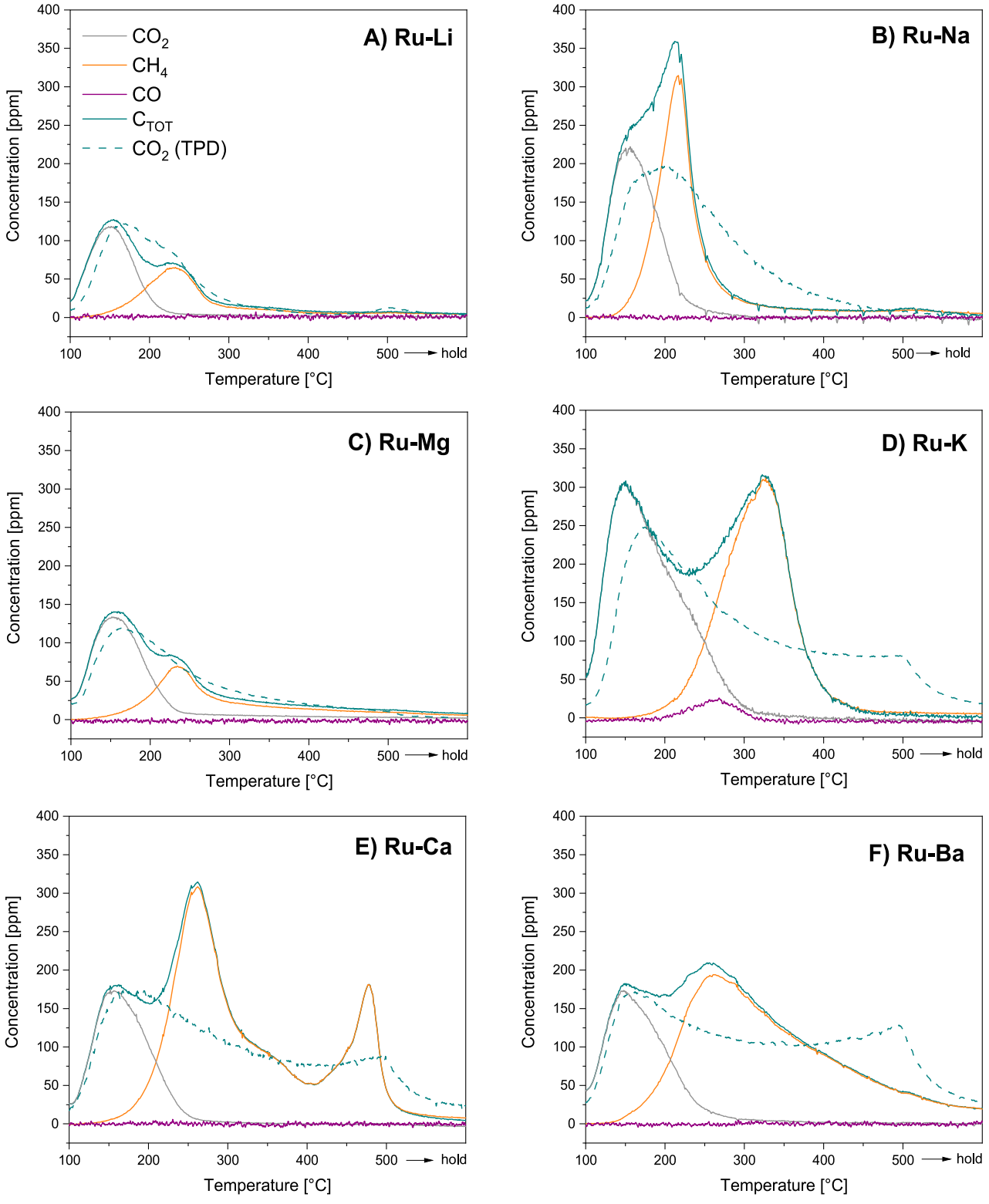

Figure 3. Concentration profiles of CO_2, CH_4, CO, and overall C profile (C_{TOT}) during H_2-TPSR tests on Ru−Li (A), Ru−Na (B), Ru−Mg (C), Ru−K (D), Ru−Ca (E), and Ru−Ba (F). The corresponding CO_2-TPD profiles (dashed lines) are reported for comparison. CO_2 preadsorption conditions: 1% CO_2/He while decreasing temperature from 500 to 100 °C (cooling rate: −5 °C/min). Heating to 500 °C at 10 °C/min in 4% H_2/He.

In absence of SM (Supporting Information, Figure S2), most of the adsorbed CO_2 desorbs upon 4% H_2 admission at 100 °C (not shown in Figure S2, see ref 10), confirming the weak adsorption of CO_2 in absence of basic sites. Most of the remaining adsorbed species are desorbed below 150 °C, where the methanation kinetics is too slow to produce appreciable amounts of CH_4. Nevertheless, a small production of CH_4 (below 15 ppm) can be observed between 150 and 400 °C.

When any SM is present, an initial CO_2 desorption feature can be observed, similar in temperature range and concen-

https://doi.org/10.1021/acs.iecr.0c05898
Ind. Eng. Chem. Res. 2021, 60, 6706−6718

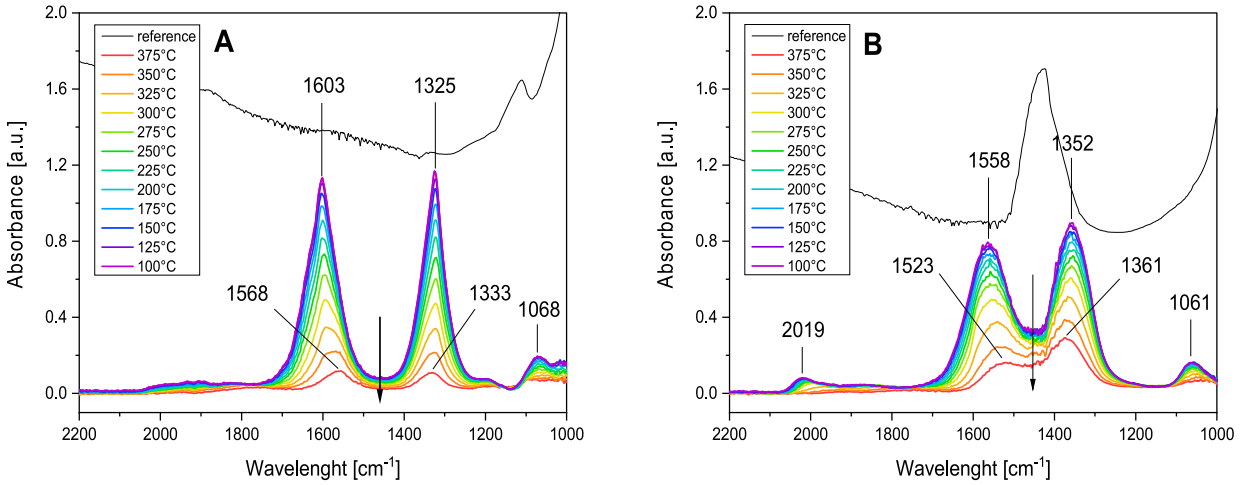

Figure 4. FT-IR spectra during H_2-TPSR on Ru−K (A) and Ru−Ba (B). CO_2 preadsorption conditions: 5 mbar of CO_2 while decreasing temperature from 375 to 100 °C (cooling rate: −5 °C/min). Heating to 375 °C at 10 °C/min in 40 mbar H_2.

tration to that observed in the case of the CO_2-TPD tests. Then, above 150 °C, the CO_2 concentration decreases, while CH_4 starts to be detected and its concentration rapidly increases with temperature, indicating the occurrence of the methanation reaction. In all cases, by comparing the C_{TOT} trace with the CO_2 trace recorded during the corresponding CO_2-TPD, a shift toward lower temperatures can be observed, indicating that the adsorbed CO_2 species react at lower temperatures if compared to the onset of their thermal desorption. This clearly indicates that the formation of CH_4 does not uniquely originate from an in-series process involving the slow thermal desorption of CO_2 from the storage sites, followed by the fast hydrogenation of the evolved CO_2 to methane over Ru. Instead, a synergistic Ru−SM interaction must be invoked to explain the accelerating effect of H_2 favoring the decomposition/hydrogenation of the adsorbed CO_2 species. The only case in which the C_{TOT} and CO_2-(TPD) traces are almost superimposed is that of Ru−Li and Ru−Mg, where apparently the methanation reaction is kinetically limited by the carbonate thermal decomposition. The enhancing effect of the presence of H_2 in the removal of the adsorbed CO_2 can also observed from a quantitative standpoint, as the total amount of C evolved during H_2-TPSR is higher than the C-evolution observed during CO_2-TPD tests (Table 1 and Figure S3).

The Ru−Na sample exhibits the narrowest peak of CH_4 among the investigated systems indicating the presence of reactive carbonates species on Na, in agreement with the literature.[25] Minor amounts of CO are detected only in the case of Ru−K, in the 200−300 °C range, peaking in between the evolution of desorbed CO_2 and produced CH_4. This evidence further confirms the intermediacy of CO in the CO_2 methanation reaction, that can be seen as a two-step reaction involving a r-WGS step producing CO and a CO-methanation step producing CH_4.[37−39] In the presence of alkaline promoters, the r-WGS step is promoted, increasing the presence of CO on the catalyst surface and facilitating the activation of CO_2.[30]

Finally, at variance to the other samples, in the case of Ru−Ca and Ru−Ba very stable carbonates are present, as pointed out by CH_4 formation even at high temperatures. This is particularly evident in the case of Ca, where two separate CH_4 peaks are observed, centered at 270 and 500 °C. These likely correspond to carbonates adsorbed with high stability, possibly on large CaO domains forming bulk $CaCO_3$ upon CO_2 adsorption.[26] Quantitatively, the samples showing more stable carbonates species also show a higher CH_4 formation during the TPSR test (Table 1): 315 μmol/g_{cat} in the case of Ru−Ca, 305 μmol/g_{cat} for Ru−Ba and 249 μmol/g_{cat} on Ru−K.

The reducibility of the adsorbed species arising from CO_2 adsorption has also been studied by FT-IR experiments for the Ru−K and Ru−Ba samples, and the results are reported in Figure 4A and B, respectively.

In agreement with the gas phase analysis, in the presence of H_2, the bands of surface carbonates decrease faster upon heating in the presence of hydrogen than under vacuum, pointing out that the hydrogenation of carbonates is favored with respect to their thermal desorption (compare Figure 2A with 4A and Figure 2B with 4B, for Ru−K and Ru−Ba samples, respectively). In line with gas phase results surface carbonates are still present in sensible amounts at 375 °C, particularly on Ru−Ba. Moreover, the high frequency envelopes centered at 1603 and 1558 cm^{-1} become less symmetric upon heating and are also red-shifted (i.e., to 1568 and 1523 cm^{-1}, respectively). Conversely, the low frequency envelopes centered at 1325 and 1352 cm^{-1} are blue-shifted to 1333 and 1361 cm^{-1}, respectively. As reported above, this effect could be explained with the different thermal stability of surface bidentate carbonates. In addition, the formation of water via the r-WGS and methanation reaction could also promote the transformation of bidentate carbonates into ionic carbonates (i.e., at ca. 1430 cm^{-1}) over Ba-based catalysts,[40] which could further justify the blue shift of bidentate carbonates.

Concerning reaction intermediates, Ru-carbonyls in the 1800−2050 range originate during the CO_2 adsorption step from the reduction of adsorbed CO_2 with residual hydrogen, as previously observed in the CO_2-TPD test. Formates are also expected as intermediate species in the CH_4 formation pathway and have been observed by means of FT-IR spectroscopy both the direct methanation of CO_2 on Ru/Al_2O_3 catalysts[24,37,41] and on the cyclic methanation on Na-Based DFMs.[36,42] However, the characteristic bands of such species are reasonably covered by the much more intense carbonates bands in the same spectral region.

3.4. Reactivity under Cyclic Conditions at 350 °C. The prepared DFMs have been tested in CO_2 capture and

https://doi.org/10.1021/acs.iecr.0c05898
Ind. Eng. Chem. Res. 2021, 60, 6706−6718

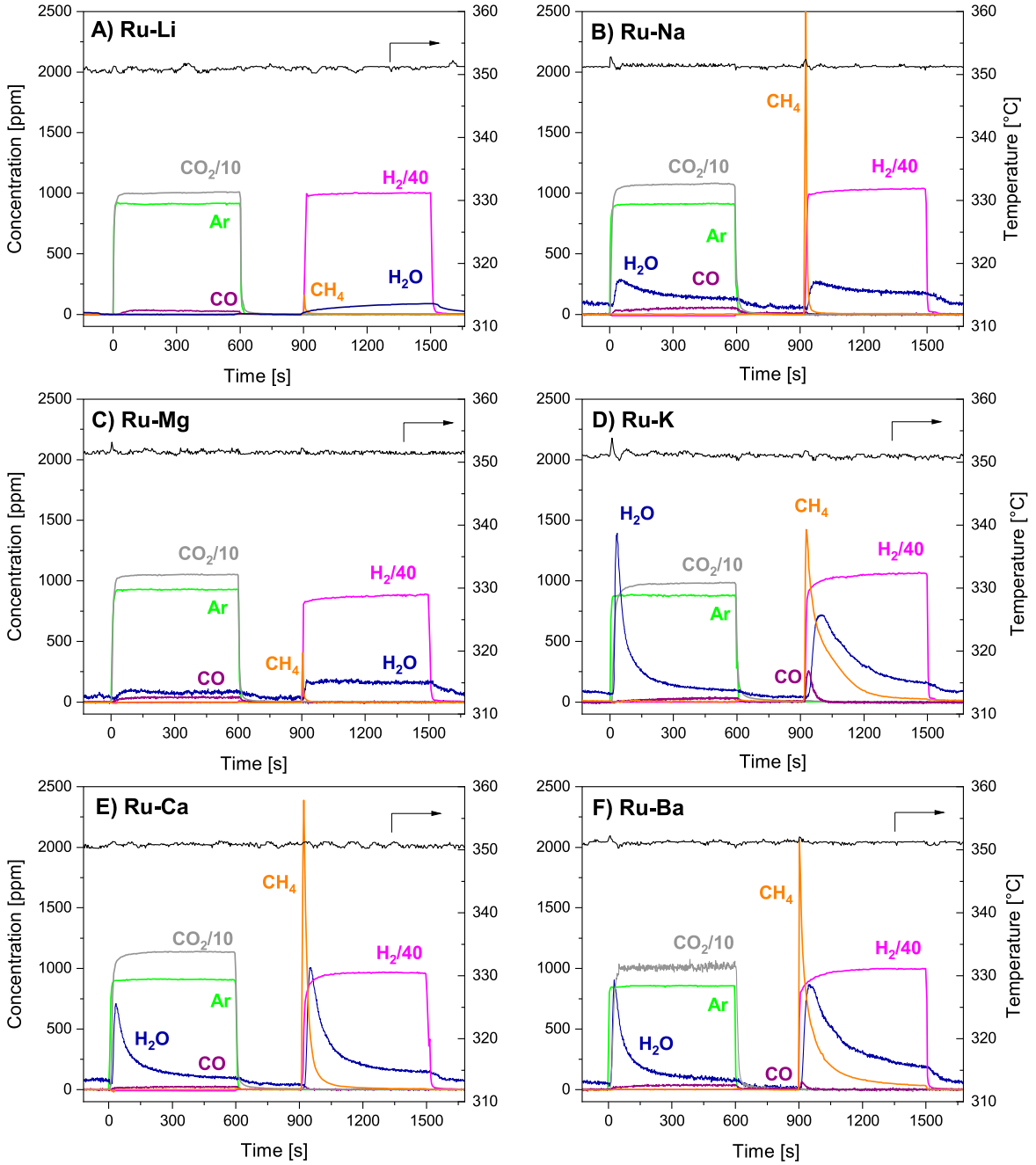

Figure 5. CO_2 capture and methanation cycles at 350 °C on Ru−Li (A), Ru−Na (B), Ru−Mg (C), Ru−K (D), Ru−Ca (E), and Ru−Ba (F). Adsorption conditions, 1% CO_2/He; reduction conditions, 4% H_2/He; flow rate, 100 mL(STP)/min.

Table 2. CO_2 Storage Capacity at 350°C, Amount of Reduction Products Formed during the Hydrogenation Phase of the Last Cycle[a]

		Ru	Ru−Li	Ru−Na	Ru−K	Ru−Mg	Ru−Ca	Ru−Ba
capture step	CO_2 adsorbed [μmol/g]	2	2	47	188	4	138	225
reduction step	CH_4 produced [μmol/g]	2	2	47	176	4	107	153
	CO produced [μmol/g]	0	0	0	11	0	1	2

[a]Process conditions as in Figure 5.

methanation cycles at 350 °C, and the results are shown in Figure 5. The quantitative amounts of CO_2 storage capacity at 350 °C and CH_4 produced per cycle are reported in Table 2.

The performance of Ru−Li (Figure 5A) is comparable to that of Ru/Al_2O_3 (shown in the Supporting Information, Figure S4). In both cases, during the CO_2 adsorption step the formation of 25 ppm of CO is observed, likely due to the occurrence of the r-WGS reaction between CO_2 from the gas phase and residual hydrogen adspecies coming from the hydrogenation phase of the previous cycle.[10,19] The negligible

https://doi.org/10.1021/acs.iecr.0c05898
Ind. Eng. Chem. Res. 2021, 60, 6706−6718

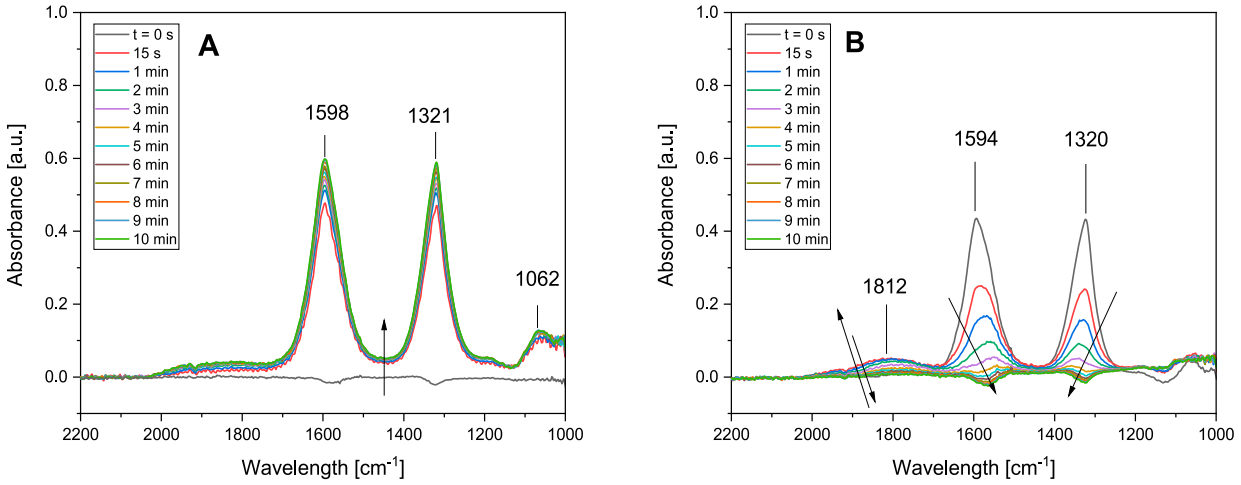

Figure 6. FT-IR spectra during CO_2 capture (A) and subsequent hydrogenation (B) at 350 °C on Ru−K. CO_2 capture conditions, 5 mbar CO_2, 10 min; hydrogenation conditions, 40 mbar H_2, 10 min.

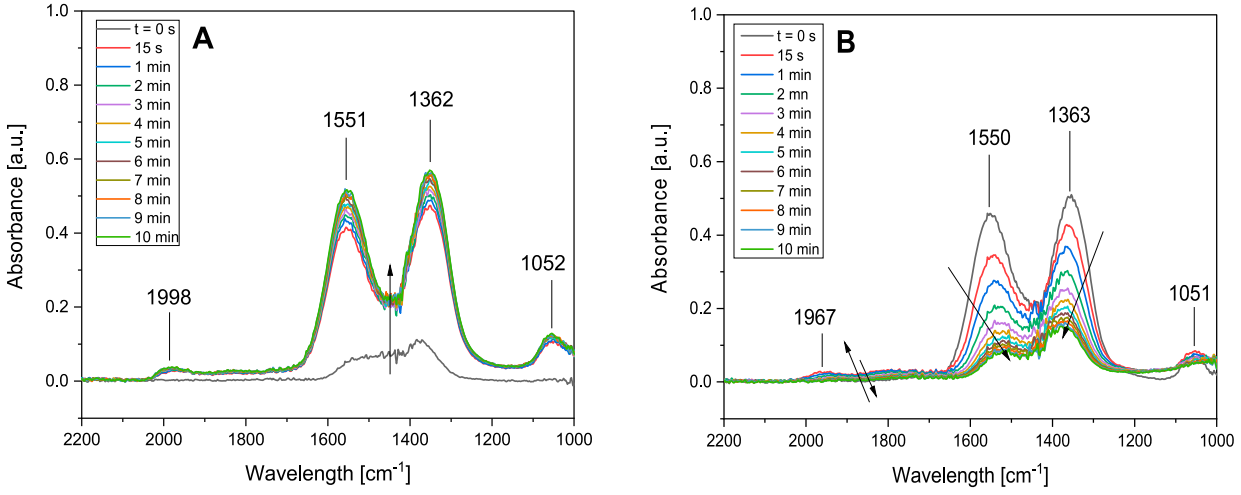

Figure 7. FT-IR spectra during CO_2 capture (A) and subsequent hydrogenation (B) at 350 °C on Ru−Ba. CO_2 capture conditions, 5 mbar CO_2, 10 min; hydrogenation conditions: 40 mbar H_2, 10 min.

formation of CH_4 upon H_2 exposure is due to the lack of CO_2 adsorbed on the samples. In fact, as anticipated from CO_2-TPD and H_2-TPSR tests, both Ru and Ru−Li samples lack adsorption sites where CO_2 can be effectively retained at 350 °C. The observed CH_4 formation likely derives from CO species formed on metallic Ru particles during the capture step, as observed by FT-IR experiments on SM-promoted samples.

In the case of Ru−Na (Figure 5B), 55 ppm of CO can also be detected during the CO_2 capture step. Upon H_2 admission, a very sharp CH_4 peak can be observed. This confirms the very fast methanation rates of weakly bound sodium carbonates, as already reported by Farrauto et al.[25] However, the amount of CH_4 produced per cycle is only 47 μmol/g_{cat} at 350 °C, and when the temperature is increased after the cycle no additional methane formation is observed, indicating a complete CO_2 removal. The amount of produced CH_4 is lower than other Na-based DFMs reported in the literature,[12,18,19,25] ranging from 178[18] to 614 μmol/g,[25] even if the comparison might not be fair due to the different process conditions and DFM formulations. It is worth to note that the reference literature materials were prepared using Na_2CO_3 as precursor salt to obtain a Na metal loading of roughly 4.3%, while in our case CH_3COONa was used to obtain 3% Na. To verify a possible role of a different Na precursor, a different Ru−Na sample was prepared starting from the Na_2CO_3 (sodium carbonate anhydrous 99.5%, Fisher Scientific) to obtain a nominal Na loading of 3%. CH_4 formation on this Ru−Na sample (ex-carbonate) (SI, Figure S5) is 98 μmol/g_{cat} per cycle, which is still less than literature values, but almost twice the corresponding amount obtained starting from the acetate precursor. This is possibly related to the different Na dispersion originating from the two different precursors and being higher in the case of the carbonate.

In the case of the Ru−Mg sample (Figure 5C), the amount of adsorbed CO_2 and produced methane is only slightly higher than that observed in absence of SM, indicating an almost negligible contribution of Mg in the storage of CO_2 in these conditions. Mg was found to be the least performing SM for DFMs also in other screening works,[18,25] and it is probably more suited for capturing CO_2 at lower temperatures.[43]

In the case of Ru−K (Figure 5D), the adsorption of CO_2 is more substantial and can be clearly observed during the adsorption phase as the signal of CO_2 is delayed with respect to that of the Ar tracer. The evolution of water is observed upon CO_2 adsorption; this is a consequence of CO_2 adsorbing

https://doi.org/10.1021/acs.iecr.0c05898
Ind. Eng. Chem. Res. 2021, 60, 6706−6718

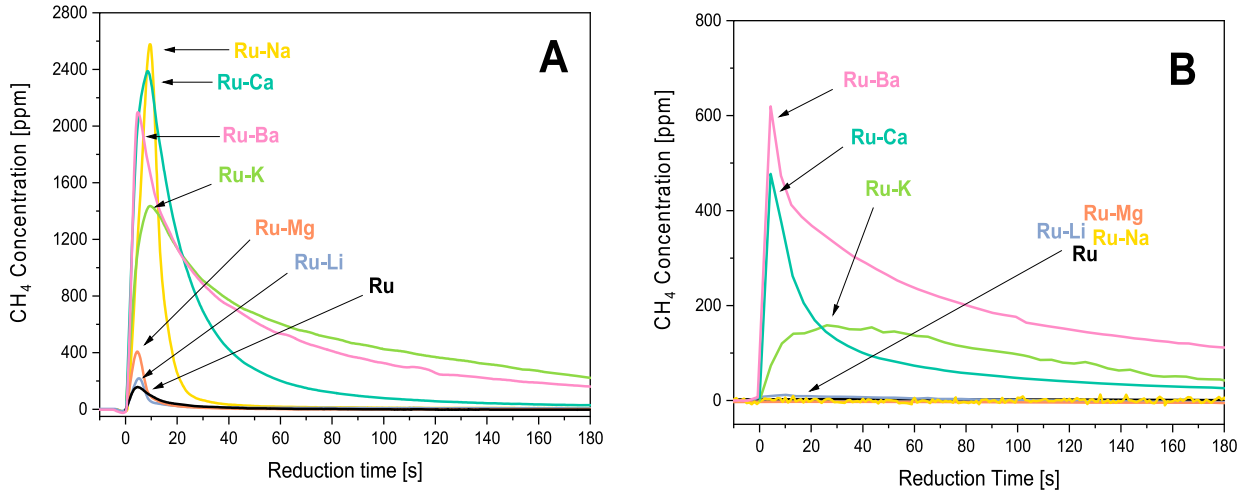

Figure 8. CH_4 evolution during the first 180 s of the hydrogenation step after CO_2 capture in the absence (A) and in the presence of O_2 and H_2O (B). Adsorption conditions, (A) 1% CO_2/He and (B) 2.5% H_2O/3% O_2/1% CO_2/He; reduction conditions, 4% H_2/He; flow rate, 100 mL(STP)/min.

Table 3. CO_2 Storage Capacity at 350°C, Amount of Reduction Products Formed during the Hydrogenation Phase of the Last Cycle[a]

		Ru	Ru−Li	Ru−Na	Ru−K	Ru−Mg	Ru−Ca	Ru−Ba
capture step	CO_2 adsorbed [μmol/g]	0	0	0	28	0	116	165
reduction step	CH_4 produced [μmol/g]	0	0	0	28	0	36	80
	CO produced [μmol/g]	0	0	0	0	0	0	0

[a]Process conditions as in Figure 8.

as carbonates at the expenses of OH groups, which are desorbed as water.[10,12] Carbonate formation is an exothermic reaction, as pointed out by the temperature increase of almost 3 °C recorded in the catalytic bed upon CO_2 admission. During the reduction phase, formation of CH_4 is observed (176 μmol/g_{cat} per cycle), accompanied by CO (11 μmol/g). Also, in this case, this value is lower with respect to literature on DFM prepared starting from K_2CO_3 precursor, with 467 μmol/g_{cat} for a sample having however Ru and K loading (5% Ru/7.1%K_2O/Al_2O_3) after exposure for 1 h with 10% H_2 at 320 °C.[25] The methane formation dynamics in this case appears slower with respect to the Ru−Na sample, as the CH_4 concentration gradually tails down and methane can be detected during the whole 10 min of H_2 exposure. This is in line with the adsorption of carbonates more strongly bound on K with respect to Na and Mg, as previously detailed in the CO_2-TPD and H_2-TPSR sections.

Finally, Ru−Ca and Ru−Ba (Figure 5E and F, respectively) show similar behavior to that of Ru−K during cycles, producing 107 and 153 μmol/g, respectively. However, at variance to the other samples, when the temperature was increased in 4% H_2 at the end of the cyclic test (not shown in the Figure), additional CH_4 formation was observed (30 and 70 μmol/g_{cat}, respectively). This indicates that not all the CO_2 adsorbed on these materials can be effectively hydrogenated during 10 min of exposure to 4% H_2, due to the high stability of the carbonates. In the case of Ca, literature value on CH_4 formation are in line with this work, considering that the amount of Ca typically used is 2 or 3 times higher and the reduction step is carried out with higher H_2 partial pressures and/or longer reduction times to boost CH_4 formation.[5,12,15,18,19]

CO_2 capture and methanation cycles at 350 °C were analyzed by FT-IR spectroscopy and representative cycles are shown in Figures 6 and 7 for Ru−K and Ru−Ba, respectively. In both cases, the FT-IR spectra recorded during the CO_2 storage (Figures 6A and 7A for Ru−K and Ru−Ba, respectively) show the formation of bidentate carbonates on K and Ba phase with characteristic bands at the 1650−1500, 1400−1250, and 1070−1000 cm^{-1} spectral regions. The concentration of such species rapidly increases until surface saturation. Minor amounts of Ru-carbonyls are also observed in the 2050−1800 cm^{-1} spectral region due to the occurrence of the r-WGS reaction between CO_2 and residual surface hydrogen (i.e., left on the surface during the previous methanation phase).

During the vacuum purge (5 min−not shown) between the adsorption and reduction step, the adsorbed carbonates are desorbed to some extent. This can be observed in Figures 6 and 7 by comparing the last adsorption spectra of the adsorption phase (t = 10 min spectra in panels A) with the corresponding spectra recorded prior to H_2 admission (t = 0 min spectra in panels B). Along with the decrease in the intensity, also a slight shift for carbonate bands is observed. This is likely ascribed to the decomposition of the less stable fraction of carbonates species. Moreover, during the vacuum purge, the Ru carbonyls formed on Ru during the adsorption step are completely removed.

Upon H_2 admission (Figures 6B and 7B for Ru−K and Ru−Ba, respectively), the progressive consumption of carbonates is observed. In line with gas-phase results, the hydrogenation is faster on Ru−K than on Ru−Ba. As matter of fact, in the case of Ru−K, the carbonates are almost completely removed after 5 min while they are still present in sensible amounts after 10 min in H_2 over Ru−Ba. In both cases, Ru-carbonyls are formed

https://doi.org/10.1021/acs.iecr.0c05898
Ind. Eng. Chem. Res. 2021, 60, 6706−6718

in the 2050−1800 cm^{-1} spectral region, reaching their maximum concentration as soon as H_2 is admitted (see first spectra recorded at 15s) then starts to decrease in intensity and eventually disappear.

3.5. Reactivity under Cyclic Conditions at 350 °C: Effect of Steam and O_2. The prepared samples have been tested at simulated flue gas conditions, i.e., in the presence of 2.5% H_2O and 3% O_2, during the CO_2 capture step. Figure 8 shows a comparison of the CH_4 peaks obtained over the various samples during the first 180 s of the hydrogenation phase (third cycle) in the absence and in the presence of steam and O_2 in the adsorption phase (Figure 8A and B, respectively). The complete third cycle performed on all samples is shown in Figures S6 and S7 in the Supporting Information, while the amounts of adsorbed CO_2 and reduction products are reported in Table 3.

In the absence of SM, neither CO_2 adsorption nor CH_4 production can be observed during the cycles (Figure S6). Also CO is not detected during the adsorption phase, likely due to the presence of O_2.

However, some thermal effects can be observed (Figure S6): in fact, when H_2O is fed to the reactor, a temperature increase of more than 5 °C is observed in the catalytic bed. This can be correlated with the hydration of the support material. Once CO_2/O_2 is fed, a second exothermic effect causing a temperature increase of 4 °C is detected. This relates to the fast oxidation of metallic Ru, the latter present on the catalyst surface because of the H_2 exposure during the previous cycle. In fact, upon H_2 admission, a temperature increase (5 °C) can be observed, associated with the fast reduction of RuO_x to Ru.[14]

Also in the case of Ru−Li, Ru−Na, and Ru−Mg, the amount of produced methane is negligible, as a result of the poor adsorption of CO_2 in these conditions. While the negligible adsorption of CO_2 on the Ru sample was expected due to the lack of SM, this is quite surprising especially in case of the Ru−Na sample, which showed remarkable adsorption performances in far more demanding conditions.[11] Slightly better performances (in terms of adsorbed CO_2 and formed CH_4) are observed for Ru−Na sample starting from carbonate precursor (Figure S8) instead of acetate.

We speculate that the different performances of the two Ru−Na samples depends on the different dispersion of Na obtained from the two different precursors. However, even the amount of CH_4 formed on both Ru−Na samples appears lower with respect to previous literature reports.[11,17] This might be attributed to the different impregnation sequence of Ru and SM. In fact, it is reported that dispersing Ru on a Ca-promoted Al_2O_3 leads to improved performances if compared to DFM prepared with a reversed impregnation order.[5] However, in the case of alkaline materials the impregnation order seem to have a small effect on the catalyst activity.[13]

The remaining Ru−SM catalysts (SM = K, Ca, Ba) are able to adsorb CO_2 from a O_2- and H_2O-containing stream, as also indicated by the water desorption upon CO_2/O_2 admission (Figure S7D−F), due to the displacement of OH groups by the more acidic carbonates.[10] Water release may also be produced by a thermal effect induced by the exothermic Ru oxidation reaction upon CO_2/O_2 addition. When CO_2/O_2 is removed from the feed and the sample is left in water vapor, a significant amount of CO_2 is desorbed. Despite the higher acidity of CO_2, water (present in a much higher amount) competes for the same adsorption sites. In any cases, part of the CO_2 remains adsorbed onto the catalyst when H_2 is admitted, resulting in a CH_4 production (see Table 2); however, these amounts are lower than the corresponding amount of CH_4 formed during cycles in the absence of steam and water. During the heating ramp in 4% H_2 after the cyclic test (not shown), the formation of some additional CH_4 is observed in the case of Ru−Ca and Ru−Ba, indicating that not all the adsorbed CO_2 can be effectively hydrogenated under isothermal conditions, in line with the behavior observed during the O_2- and H_2O-free cycles.

Notably, the presence of steam and O_2 during the adsorption phase results in a loss of CO_2 storage capacity at 350 °C (compare Tables 2 and 3). At the investigated metal loadings and process conditions, lighter metals such as Na and Mg are very strongly affected by the presence of oxygen and water in the adsorption feed, since negligible amounts of CO_2 has been observed to be adsorbed. By comparing the amounts of formed CH_4 during the cycles carried out in presence and in absence of O_2 and H_2O, a reduction of 84% has been observed for Ru−K, 65% for Ru−Ca, and 47% in the case of Ru−Ba. These data indicate that as the molar weight of the SMs increases and the strength of the adsorbed carbonates increases, the presence of O_2 and water is less affecting the amount of CO_2 adsorbed and therefore the CH_4 formed during the reduction step.

Preliminary results obtained from FT-IR characterization during adsorption/reduction cycles in the presence of O_2 and water indicate that the lower amount of stored CO_2 can be ascribed to the competition between water and CO_2 for the same adsorption sites and to the modification of the adsorbed CO_2 species over the hydrated surface.

In the experimental campaign of this screening work, no indication of deactivation phenomena was observed, but it is worth noting that the exposure to O_2 and H_2O was limited in terms of concentrations and number of cycles with respect to the envisioned DFM application, and the long-term stability of these DFM formulations is still to be addressed.

4. CONCLUSIONS

The reactivity of selected alkaline (Li, Na, K) and alkaline-earth (Mg, Ca, Ba) metal oxides in Ru-based DFM formulations has been analyzed in CO_2 storage and reduction to methane according to the cyclic CO_2 capture and methanation process. The prepared materials were characterized by BET, methanation reactivity, and CO_2 adsorption/reactivity (CO_2-TPD and H_2-TPSR), while the capture/methanation performance of the samples was investigated by cycles at 350 °C, with and without water and O_2 in the adsorption feed. On selected samples, the nature of the adsorbed CO_2 species was analyzed by in situ FT-IR spectroscopy.

The K-, Ca-, or Ba- containing DFMs adsorbed the highest amounts of CO_2, in the form of carbonates with high thermal stability. In the presence of H_2, carbonates arising from CO_2 adsorption can be hydrogenated to CH_4 at lower temperatures if compared to their thermal desorption in inert atmosphere. This clearly indicates that the formation of CH_4 does not uniquely originate from an in-series process involving the slow thermal desorption of CO_2 from the storage sites, followed by the fast hydrogenation of the evolved CO_2 to methane over Ru. Instead, a synergistic Ru−SM interaction must be invoked to explain the accelerating effect of H_2.

https://doi.org/10.1021/acs.iecr.0c05898
Ind. Eng. Chem. Res. 2021, 60, 6706−6718

Significant amounts of CH_4 during cyclic capture and methanation tests at 350 °C were produced only in the presence of SMs able to form stable carbonates upon CO_2 adsorption, leading to the following order of reactivity in terms of CH_4 production: Ru−K ≥ Ru−Ba > Ru−Ca > Ru−Na ≫ Ru−Mg ≅ Ru−Li ≅ Ru.

The presence of steam and O_2 during the capture step has a detrimental effect on the CO_2 adsorption and CH_4 production for all the samples; in particular, alkaline SMs are more affected than alkaline-earth ones. The decrease in the CO_2 storage capacity can be related to the competition of CO_2 and water for the same adsorption sites. Thus, SMs forming strongly bound carbonates can adsorb significant amounts of CO_2 also in the presence of water. This calls for specific DFMs formulation having a proper selection of the SM in terms of the nature and loading where a trade-off between thermal stability and reactivity should be attained in order to maximize the amounts of stored and reducible CO_2 in the presence of water and oxygen.

■ ASSOCIATED CONTENT

Supporting Information

The Supporting Information is available free of charge at https://pubs.acs.org/doi/10.1021/acs.iecr.0c05898.

Cofeeding test-results; bar graph of CO_2-TPD and H_2-TPSR results; H_2-TPSR and CO_2 capture/methanation cycles on Ru/Al_2O_3 sample; CO_2 capture/methanation cycles on Ru−Na DFM prepared from the carbonate precursor; CO_2 capture/methanation cycles on all samples with O_2 and H_2O in the adsorption feed (PDF)

■ AUTHOR INFORMATION

Corresponding Author

Luca Lietti − *Dipartimento di Energia, Politecnico Di Milano, Milano 20156, Italy;* orcid.org/0000-0002-2888-9708; Email: luca.lietti@polimi.it

Authors

Alessandro Porta − *Dipartimento di Energia, Politecnico Di Milano, Milano 20156, Italy*

Roberto Matarrese − *Dipartimento di Energia, Politecnico Di Milano, Milano 20156, Italy*

Carlo Giorgio Visconti − *Dipartimento di Energia, Politecnico Di Milano, Milano 20156, Italy;* orcid.org/0000-0001-5205-982X

Lidia Castoldi − *Dipartimento di Energia, Politecnico Di Milano, Milano 20156, Italy*

Complete contact information is available at: https://pubs.acs.org/10.1021/acs.iecr.0c05898

Notes

The authors declare no competing financial interest.

■ REFERENCES

(1) IEA. *World Energy Outlook 2017*; OECD Publishing: Paris, 2017.

(2) Blunden, J.; Arndt, D. S. State of the Climate in 2018. *Bull. Am. Meteorol. Soc.* **2019**, *100* (9), Si−S306.

(3) IEA. *Renewables 2019*. https://www.iea.org/reports/renewables-2019 (accessed 2020-11-30).

(4) Mondal, M. K.; Balsora, H. K.; Varshney, P. Progress and Trends in CO2 Capture/Separation Technologies: A Review. *Energy* **2012**, *46* (1), 431−441.

(5) Duyar, M. S.; Treviño, M. A. A.; Farrauto, R. J. Dual Function Materials for CO 2 Capture and Conversion Using Renewable H 2. *Appl. Catal., B* **2015**, *168−169*, 370−376.

(6) Farrauto, R. J.; Duyar, M. S.; Park, A. A. Methods, Systems and Materials for Capturing Carbon Dioxide and Converting It to a Chemical Product. WO 2016/007825 A1, 2016.

(7) Melo Bravo, P.; Debecker, D. P. Combining CO2 Capture and Catalytic Conversion to Methane. *Waste Dispos. Sustain. Energy* **2019**, *1* (1), 53−65.

(8) Tsiotsias, A. I.; Charisiou, N. D.; Yentekakis, I. V.; Goula, M. A. The Role of Alkali and Alkaline Earth Metals in the CO2Methanation Reaction and the Combined Capture and Methanation of CO2. *Catalysts* **2020**, *10* (7), 812.

(9) Omodolor, I. S.; Otor, H. O.; Andonegui, J. A.; Allen, B. J.; Alba-Rubio, A. C. Dual-Function Materials for CO 2 Capture and Conversion: A Review. *Ind. Eng. Chem. Res.* **2020**, *59* (40), 17612−17631.

(10) Porta, A.; Visconti, C. G.; Castoldi, L.; Matarrese, R.; Jeong-Potter, C.; Farrauto, R.; Lietti, L. Ru-Ba Synergistic Effect in Dual Functioning Materials for Cyclic CO2 Capture and Methanation. *Appl. Catal., B* **2021**, *283*, 119654.

(11) Wang, S.; Farrauto, R. J.; Karp, S.; Jeon, J. H.; Schrunk, E. T. Parametric, Cyclic Aging and Characterization Studies for CO_2 Capture from Flue Gas and Catalytic Conversion to Synthetic Natural Gas Using a Dual Functional Material (DFM). *J. CO2 Util.* **2018**, *27* (July), 390−397.

(12) Bermejo-López, A.; Pereda-Ayo, B.; González-Marcos, J. A.; González-Velasco, J. R. Mechanism of the CO2 Storage and in Situ Hydrogenation to CH4. Temperature and Adsorbent Loading Effects over Ru-CaO/Al2O3 and Ru-Na2CO3/Al2O3 Catalysts. *Appl. Catal., B* **2019**, *256* (April), 117845.

(13) Cimino, S.; Boccia, F.; Lisi, L. Effect of Alkali Promoters (Li, Na, K) on the Performance of Ru/Al2O3 Catalysts for CO2 Capture and Hydrogenation to Methane. *J. CO2 Util.* **2020**, *37*, 195−203.

(14) Wang, S.; Schrunk, E. T.; Mahajan, H.; Farrauto, R. J. The Role of Ruthenium in CO2 Capture and Catalytic Conversion to Fuel by Dual Function Materials (DFM). *Catalysts* **2017**, *7* (12), 88.

(15) Duyar, M. S.; Wang, S.; Arellano-Treviño, M. A.; Farrauto, R. J. CO 2 Utilization with a Novel Dual Function Material (DFM) for Capture and Catalytic Conversion to Synthetic Natural Gas: An Update. *J. CO2 Util.* **2016**, *15*, 65−71.

(16) Rönsch, S.; Schneider, J.; Matthischke, S.; Schlüter, M.; Götz, M.; Lefebvre, J.; Prabhakaran, P.; Bajohr, S. Review on Methanation - From Fundamentals to Current Projects. *Fuel* **2016**, *166*, 276−296.

(17) Arellano-Treviño, M. A.; Kanani, N.; Jeong-Potter, C. W.; Farrauto, R. J. Bimetallic Catalysts for CO2 Capture and Hydrogenation at Simulated Flue Gas Conditions. *Chem. Eng. J.* **2019**, *375*, 121953.

(18) Chai, K. H.; Leong, L. K.; Wong, D. S. H.; Tsai, D. H.; Sethupathi, S. Effect of CO2 Adsorbents on the Ni-Based Dual-Function Materials for CO2 Capturing and in Situ Methanation. *J. Chin. Chem. Soc.* **2020**, *67* (6), 998−1008.

(19) Bermejo-López, A.; Pereda-Ayo, B.; González-Marcos, J. A.; González-Velasco, J. R. Ni Loading Effects on Dual Function Materials for Capture and In-Situ Conversion of CO2 to CH4 Using CaO or Na2CO3. *J. CO2 Util.* **2019**, *34*, 576−587.

(20) Sun, H.; Zhang, Y.; Guan, S.; Huang, J.; Wu, C. Direct and Highly Selective Conversion of Captured CO2 into Methane through Integrated Carbon Capture and Utilization over Dual Functional Materials. *J. CO2 Util.* **2020**, *38* (January), 262−272.

(21) Porta, A.; Falbo, L.; Visconti, C. G.; Lietti, L.; Bassano, C.; Deiana, P. Synthesis of Ru-Based Catalysts for CO2Methanation and Experimental Assessment of Intraporous Transport Limitations. *Catal. Today* **2020**, *343* (October 2018), 38−47.

(22) Castoldi, L.; Nova, I.; Lietti, L.; Forzatti, P. Study of the Effect of Ba Loading for Catalytic Activity of Pt-Ba/Al 2O3Model Catalysts. *Catal. Today* **2004**, *96* (1−2), 43−52.

(23) Lindholm, A.; Currier, N. W.; Dawody, J.; Hidayat, A.; Li, J.; Yezerets, A.; Olsson, L. The Influence of the Preparation Procedure

on the Storage and Regeneration Behavior of Pt and Ba Based NOx Storage and Reduction Catalysts. *Appl. Catal., B* **2009**, *88* (1−2), 240−248.
(24) Wang, X.; Hong, Y.; Shi, H.; Szanyi, J. Kinetic Modeling and Transient DRIFTS-MS Studies of CO2Methanation over Ru/Al2O3 Catalysts. *J. Catal.* **2016**, *343*, 185−195.
(25) Arellano-Treviño, M. A.; He, Z.; Libby, M. C.; Farrauto, R. J. Catalysts and Adsorbents for CO2 Capture and Conversion with Dual Function Materials: Limitations of Ni-Containing DFMs for Flue Gas Applications. *J. CO2 Util.* **2019**, *31*, 143−151.
(26) Gruene, P.; Belova, A. G.; Yegulalp, T. M.; Farrauto, R. J.; Castaldi, M. J. Dispersed Calcium Oxide as a Reversible and Efficient CO 2 -Sorbent at Intermediate Temperatures. *Ind. Eng. Chem. Res.* **2011**, *50* (7), 4042−4049.
(27) Prinetto, F.; Manzoli, M.; Morandi, S.; Frola, F.; Ghiotti, G.; Castoldi, L.; Lietti, L.; Forzatti, P. Pt-K/Al 2 O 3 NSR Catalysts: Characterization of Morphological, Structural and Surface Properties. *J. Phys. Chem. C* **2010**, *114* (2), 1127−1138.
(28) Hadjiivanov, K.; Lavalley, J. C.; Lamotte, J.; Maugé, F.; Saint-Just, J.; Che, M. FTIR Study of CO Interaction with Ru/TiO2 Catalysts. *J. Catal.* **1998**, *176* (2), 415−425.
(29) Panagiotopoulou, P.; Verykios, X. E. Mechanistic Study of the Selective Methanation of CO over Ru/TiO 2 Catalysts: Effect of Metal Crystallite Size on the Nature of Active Surface Species and Reaction Pathways. *J. Phys. Chem. C* **2017**, *121* (9), 5058−5068.
(30) Panagiotopoulou, P. Methanation of CO2 over Alkali-Promoted Ru/TiO2 Catalysts: II. Effect of Alkali Additives on the Reaction Pathway. *Appl. Catal., B* **2018**, *236* (March), 162−170.
(31) Wang, X.; Shi, H.; Kwak, J. H.; Szanyi, J. Mechanism of CO 2 Hydrogenation on Pd/Al 2 O 3 Catalysts: Kinetics and Transient DRIFTS-MS Studies. *ACS Catal.* **2015**, *5* (11), 6337−6349.
(32) Castoldi, L.; Lietti, L.; Nova, I.; Matarrese, R.; Forzatti, P.; Vindigni, F.; Morandi, S.; Prinetto, F.; Ghiotti, G. Alkaline- and Alkaline-Earth Oxides Based Lean NOx Traps: Effect of the Storage Component on the Catalytic Reactivity. *Chem. Eng. J.* **2010**, *161* (3), 416−423.
(33) Frola, F.; Prinetto, F.; Ghiotti, G.; Castoldi, L.; Nova, I.; Lietti, L.; Forzatti, P. Combined in Situ FT-IR and TRM Analysis of the NOx Storage Properties of Pt-Ba/Al2O3 LNT Catalysts. *Catal. Today* **2007**, *126* (1−2), 81−89.
(34) Frola, F.; Manzoli, M.; Prinetto, F.; Ghiotti, G.; Castoldi, L.; Lietti, L. Pt-Ba/Al 2 O 3 NSR Catalysts at Different Ba Loading: Characterization of Morphological, Structural, and Surface Properties. *J. Phys. Chem. C* **2008**, *112* (33), 12869−12878.
(35) Chin, S. Y.; Williams, C. T.; Amiridis, M. D. FTIR Studies of CO Adsorption on Al2O3- and SiO 2-Supported Ru Catalysts. *J. Phys. Chem. B* **2006**, *110* (2), 871−882.
(36) Proaño, L.; Tello, E.; Arellano-Trevino, M. A.; Wang, S.; Farrauto, R. J.; Cobo, M. In-Situ DRIFTS Study of Two-Step CO2 Capture and Catalytic Methanation over Ru,"Na2O"/Al2O3 Dual Functional Material. *Appl. Surf. Sci.* **2019**, *479*, 25−30.
(37) Falbo, L.; Visconti, C. G.; Lietti, L.; Szanyi, J. The Effect of CO on CO2Methanation over Ru/Al2O3 Catalysts: A Combined Steady-State Reactivity and Transient DRIFT Spectroscopy Study. *Appl. Catal., B* **2019**, *256*, 117791.
(38) Zhao, K.; Wang, L.; Calizzi, M.; Moioli, E.; Züttel, A. In Situ Control of the Adsorption Species in CO2 Hydrogenation: Determination of Intermediates and Byproducts. *J. Phys. Chem. C* **2018**, *122* (36), 20888−20893.
(39) Mutschler, R.; Moioli, E.; Zhao, K.; Lombardo, L.; Oveisi, E.; Porta, A.; Falbo, L.; Visconti, C. G.; Lietti, L.; Züttel, A. Imaging Catalysis: Operando Investigation of the CO 2 Hydrogenation Reaction Dynamics by Means of Infrared Thermography. *ACS Catal.* **2020**, *10* (3), 1721−1730.
(40) Morandi, S.; Prinetto, F.; Ghiotti, G.; Castoldi, L.; Lietti, L.; Forzatti, P.; Daturi, M.; Blasin-Aubé, V. The Influence of CO2 and H2O on the Storage Properties of Pt-Ba/Al2O3 LNT Catalyst Studied by FT-IR Spectroscopy and Transient Microreactor Experiments. *Catal. Today* **2014**, *231* (2), 116−124.
(41) Zhao, K.; Wang, L.; Moioli, E.; Calizzi, M.; Züttel, A. Identifying Reaction Species by Evolutionary Fitting and Kinetic Analysis: An Example of CO 2 Hydrogenation in DRIFTS. *J. Phys. Chem. C* **2019**, *123* (14), 8785−8792.
(42) Proaño, L.; Arellano-Treviño, M. A.; Farrauto, R. J.; Figueredo, M.; Jeong-Potter, C.; Cobo, M. Mechanistic Assessment of Dual Function Materials, Composed of Ru-Ni, Na2O/Al2O3 and Pt-Ni, Na2O/Al2O3, for CO2 Capture and Methanation by in-Situ DRIFTS. *Appl. Surf. Sci.* **2020**, *533* (July), 147469.
(43) Wu, K.; Ye, Q.; Wu, R.; Chen, S.; Dai, H. Carbon Dioxide Adsorption Behaviors of Aluminum-Pillared Montmorillonite-Supported Alkaline Earth Metals. *J. Environ. Sci. (Beijing, China)* **2020**, *98*, 109−117.

https://doi.org/10.1021/acs.iecr.0c05898
Ind. Eng. Chem. Res. 2021, 60, 6706−6718